

# Towards Panoptic 3D Parsing for Single Image in the Wild

Sainan Liu<sup>1,2</sup> Vincent Nguyen<sup>1</sup> Yuan Gao<sup>1</sup> Subarna Tripathi<sup>2</sup> Zhuowen Tu<sup>1</sup>  
<sup>1</sup>UC San Diego <sup>2</sup>Intel Labs

{sall131, vvn012, ylgao, ztu}@ucsd.edu, {sainan.liu, subarna.tripathi}@intel.com

## Abstract

Performing single image holistic understanding and 3D reconstruction is a central task in computer vision. This paper presents an integrated system that performs dense scene labeling, object detection, instance segmentation, depth estimation, 3D shape reconstruction, and 3D layout estimation for indoor and outdoor scenes from a single RGB image. We name our system panoptic 3D parsing (Panoptic3D) in which panoptic segmentation (“stuff” segmentation and “things” detection/segmentation) with 3D reconstruction is performed. We design a stage-wise system, Panoptic3D (stage-wise), where a complete set of annotations is absent. Additionally, we present an end-to-end pipeline, Panoptic3D (end-to-end), trained on a synthetic dataset with a full set of annotations. We show results on both indoor (3D-FRONT) and outdoor (COCO and Cityscapes) scenes. Our proposed panoptic 3D parsing framework points to a promising direction in computer vision. Panoptic3D can be applied to a variety of applications, including autonomous driving, mapping, robotics, design, computer graphics, robotics, human-computer interaction, and augmented reality.

## 1. Introduction

One of the main objectives in computer vision is to develop systems that can “see” the world [36, 49]. Here we tackle the problem of single image holistic understanding and 3D reconstruction, which is deeply rooted in decades of development in computer vision and photogrammetry but became practically feasible only recently thanks to the exploding growth in modeling, computing [16, 21, 27, 45, 47, 56], and large-scale datasets [5, 10, 12, 14, 32].

We name our system single image panoptic 3D parsing (Panoptic3D). It takes in a single natural RGB image and jointly performs dense image semantic labeling [34, 44, 50], object detection [41], instance segmentation [20], depth estimation [1, 30], object shape 3D reconstruction [15, 61], and 3D layout estimation [52] from a single natural RGB image. Figure 1 gives an illustration for the pipeline where a 3D

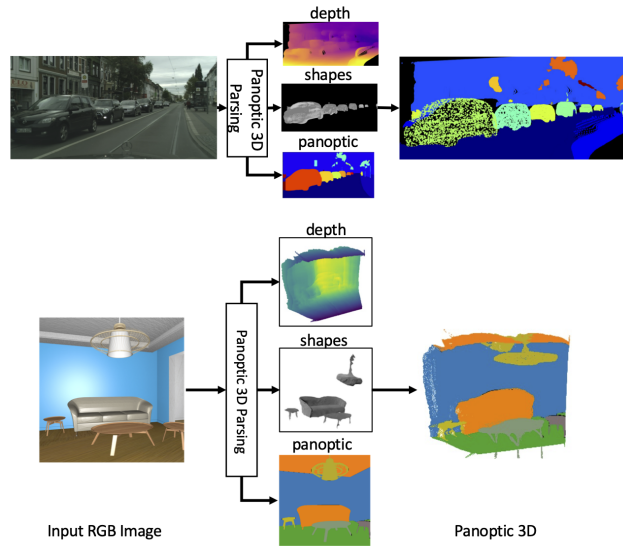


Figure 1. Our stage-wise Panoptic 3D Parsing System (Panoptic3D), shown in the first row, takes a single-view image as input and outputs panoptic 3D results, a scene reconstruction with “stuff” and “things” shown on the right-hand side. The stage-wise pipeline works on natural image datasets where complete ground-truth annotations for segmentation and 3D reconstruction are absent, such as COCO [32] and Cityscapes [10] where ground-truth 3D reconstruction is missing in both training and evaluation. The second row shows an alternative end-to-end model, Panoptic3D (end-to-end) applied to the synthetic 3D-FRONT [14] dataset.

scene is estimated from a single-view RGB image with the background layout (“stuff”) segmented and the individual foreground instances (“things”) detected, segmented, and fully reconstructed. A closely related work to our Panoptic3D is the recent Total3DUnderstanding method [38] where 3D layout and instance 3D meshes are reconstructed for an indoor input image. However, Total3DUnderstanding [38] does not perform panoptic segmentation [25]/image parsing [51] and is limited to indoor scenes.

We briefly discuss the literature from two main angles: 1). 3D reconstruction, particularly from a single-view RGB image; and 2). image understanding, particularly for panoptic segmentation [25] and image parsing [51].

Table 1. Comparison for different 3D reconstruction methods. Mesh-RCNN [15] only allows single-instance per image during training, but it will enable outputs of multi-object components at inference time. Nevertheless, efforts are still required to allow for the multi-object module in an end-to-end pipeline for training and evaluation.

Method	3D	Single image	Layout 3D	Panoptic segmentation	Outdoor scenes	Multiple objects
[17, 23, 58, 61]	✓	✓				
[15]	✓	✓				†
[18]	✓	✓			✓	
[22, 38, 52, 62]	✓	✓	✓			✓
[30]	✓	✓			✓	
[1]	✓	✓	✓		✓	
[39, 40]	✓		✓		✓	✓
[24, 25, 29, 57]		✓		✓	✓	✓
Panoptic3DParsing (ours)	✓	✓	✓	✓	✓	✓

3D reconstruction is an important area in photogrammetry [8, 33] and computer vision [4, 19, 28, 35, 39, 40, 48, 53]. We limit our scope to single RGB image input for 3D instance reconstruction [6, 17, 23, 54, 55, 58, 61] and 3D layout generation [52, 62]. There is a renewed interest in performing holistic image and object segmentation (Image Parsing [51]), called panoptic segmentation [24, 25, 29, 57], where the background regions (“stuff”) are labeled with the foreground objects (“things”) detected. Our panoptic 3D parsing method is a system that gives holistic 3D scene reconstruction and understanding for an input image. It includes multiple tasks such as depth estimation, panoptic segmentation, and object instance reconstruction.

In Section 2, we discuss the motivations for the individual modules. A comparison between the existing methods and ours is illustrated in Table 1. The contributions of our work are summarized below.

- We present a stage-wise system for panoptic 3D parsing, Panoptic3D (stage-wise), by combatting the issue where full annotations for panoptic segmentation, depth, and 3D instances are absent. To the best of our knowledge, this is the first system of its kind to perform joint panoptic segmentation and holistic 3D reconstruction for the generic indoor and outdoor scenes from a single RGB image.
- In addition, we have developed an end-to-end pipeline for panoptic 3D parsing, Panoptic3D (end-to-end), where datasets have complete segmentation and 3D reconstruction ground-truth annotations.

Observing the experiments, we show encouraging results for indoor [14] and the outdoor scenes for the natural scenes [10, 32].

## 2. Related Work

Table 1 shows a comparison with related work. Our panoptic 3D parsing framework has the most complete set

of properties and is more general than the competing methods. Next, we discuss related work below in details.

**Single-view 3D scene reconstruction.** Single image 3D reconstruction has a long history [18, 22, 38, 42, 52, 62]. The work in [22] jointly predicts 3D layout bounding box, 3D object bounding box, and camera intrinsics without any geometric reconstruction for indoor scenes. Factored3D [52] is closely related to our work, which combines indoor scene layout (amodal depth) with 3D instance reconstructions without much abstraction. Still, no label is predicted for the scene layout (“stuff”) [52], and the instance object reconstruction tends to overfit the canonical shape of known categories. Total3DUnderstanding [38] infers a box layout and has produced 3D reconstruction inference results on natural indoor images. However, as discussed before, these methods do not perform holistic 3D reconstruction for natural outdoor scenes or panoptic segmentation in general.

**Single image depth estimation.** David Marr pioneered the 2.5D depth representation [36]. Depth estimation from a single image can be performed in a supervised way and has been extensively studied in the literature [13, 43]. Development in deep learning [34] has expedited the progress for depth estimation [3, 30]. In our work, we adopt a relatively lightweight inverse depth prediction module from Factored3D [52] and regress the loss jointly with 3D reconstruction and panoptic segmentation.

**Single-view single object reconstruction.** Single image single object 3D reconstruction can typically be divided into volume-based [6, 55, 61], mesh-based [17, 23, 54], and implicit-function-based [7, 58] methods. In this paper, we adopt the detection and shape reconstruction branch from Mesh R-CNN [15] for multi-object prediction. Building on top of it, we can perform supervised end-to-end single image panoptic 3D parsing. We also adopt unseen class reconstruction, GenRe [61], for multi-object reconstruction for natural image reconstruction when well-aligned ground truth 3D mesh models are not available.

**Panoptic and instance segmentation.** Panoptic segmenta-

tion [25] or image parsing [51] combines semantic segmentation and instance detection/segmentation. In our work, we build our panoptic head by referencing the end-to-end structure of UPSNet [57]. Additionally, we predict the 3D reconstruction of instances for each corresponding instance mask. However, the instance segmentation in panoptic segmentation is occluded. In comparison, amodal instance segmentation predicts un-occluded instance masks for “things”. In this work, we generate both amodal as well as panoptic segmentation annotations from the 3D-FRONT dataset. This dataset enables the network to jointly perform 3D “things” reconstruction as well as panoptic segmentation. In the stage-wise pipeline, we utilize the work from Zhan *et al.* [60] to better assist 3D reconstruction on natural images.

### 3. Method

We design our networks with the following goals in mind: 1). The network should be generalizable to both indoor and outdoor environments; 2). Datasets with various levels of annotations should be able to utilize the framework with simple replacement; 3). The segmentation masks should align with the reconstruction from the input view.

We will first introduce our stage-wise system, Panoptic3D (stage-wise) and show that it can process natural images without corresponding 3D annotations in training. Then, we will present our end-to-end network, Panoptic3D (end-to-end).

#### 3.1. Stage-wise Panoptic3D

We present our stage-wise system, Panoptic3D (stage-wise), in Figure 2. We design this system for natural image datasets that contain well-annotated panoptic segmentation information but lack 3D information, such as COCO [32] and Cityscapes [10]. This stage-wise system contains four main parts: 1). Instance and panoptic segmentation network. 2). Instance amodal completion network. 3). Single object 3D reconstruction network for unseen classes. 4). Single-image depth prediction network.

We take advantage of the state-of-art panoptic segmentation system, UPSNet [57], scene de-occlusion system [60], depth prediction system, DenseDepth [1], and unseen class object reconstruction networks [61] and integrate them into a single pipeline.

This Panoptic3D (stage-wise) framework takes an RGB image and predicts the panoptic 3D parsing of the scene in point cloud (for “stuff”) and meshes (for “things”). The implementation details are as follows: the network first takes panoptic results from UPSNet and depth estimation from DenseDepth. It then passes the modal masks to the de-occlusion net to acquire amodal masks. We use GenRe to reconstruct the instance meshes based on the amodal masks. The module then maps panoptic labels to depth pixels and

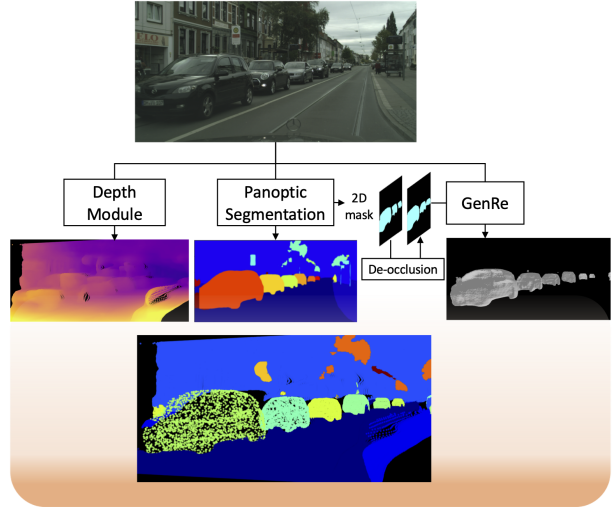


Figure 2. Our stage-wise system, Panoptic3D (stage-wise). We adopt DenseDepth [1] for depth prediction, UPSNet [57] for panoptic segmentation, a de-occlusion network [60] for amodal mask completion, and GenRe [61] to perform instance-based single image 3D reconstruction. The alignment module in Panoptic3D (stage-wise) outputs the image on the bottom.

uses empirically estimated camera intrinsics estimation to inverse project depth into point clouds.

Since GenRe [61] only predicts normalized meshes centering at the origin, the final module aligns individual shapes using depth estimation in the z-direction and the mask in the x-y direction. The module takes the mean of the 98th percentile and the 2nd percentile of the filtered and sorted per-pixel depth prediction within the predicted mask region to estimate the z center depth of each object. Finally, it places meshes and depth point cloud in the same coordinate system to render the panoptic 3D parsing results. The general inference time is 2.4 seconds per image on one NVIDIA Titan X GPU.

#### 3.2. End-to-end Panoptic3D

The overview of the end-to-end network structure, Panoptic3D (end-to-end), is shown in Figure 3. Similar to Panoptic3D (stage-wise), Panoptic3D (end-to-end) also has four main components: 1). instance segmentation head. 2). multi-object training enabled shape heads. 3). panoptic segmentation head. 4). “stuff” depth and relative object z center prediction branch. The entire network is trained end-to-end and can jointly predict amodal instance, semantic, and panoptic segmentation, “stuff” depth, and “things” reconstruction in 3D. Our design ideas are as follows.

For the panoptic 3D prediction, we predict “stuff” depth instead of box representation because it is not easily generalizable to scenes with other “stuff” categories, such as windows, doors, rugs, etc., and it does not apply to out-

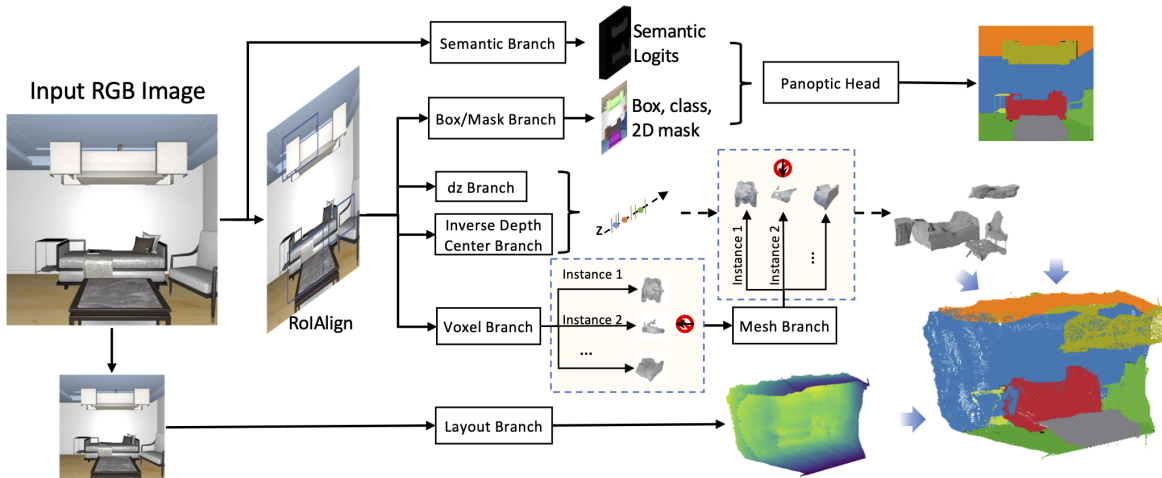


Figure 3. Network architecture for our Panoptic3D (end-to-end) pipeline. dz: means depth extent. The red stop sign indicates that only predictions with centered ground truth shapes are used for regression during training.

door environments. Taking advantage of the advanced development in 2D panoptic segmentation, we first predict 2D panoptic segmentation and then align “stuff” segmentation with the depth prediction.

We predict that amodal “stuff” prediction would significantly improve the panoptic 3D parsing task for future works.

For multi-object 3D reconstruction, we first enable multi-object training and evaluation for the baseline network. For joint training with panoptic segmentation, we mainly address the following three challenges: 1). With multiple objects in a scene, mesh shapes that are too close to the camera may have a negative z-center, not tolerated in end-to-end detection and reconstruction baseline model by design. 2). For objects that appear to be cut-off by the camera view (non-centered/boundary objects) or too close to the camera, transformation to camera coordinate will deform ground truth 3D voxel and mesh into a shape that contain infinitely far points, preventing the network from converging. One approach would be to cut the ground truth shapes to be within the camera frustum. However, this may result in unnatural edge connections, and the preprocessing step is time-consuming. Instead, we introduce a partial loss. We first detect and mark objects occluded by image boundaries (non-centered/boundary objects) and exclude their loss for shape-related regressions. For example, we use an indicator function  $\mathbb{1}(\cdot)$  to return 1 for centered objects and 0 for boundary objects. The final loss per batch is defined as  $\mathcal{L} = \mathcal{L}_{mask} [20] + \mathcal{L}_{box} [20] + \mathcal{L}_{class} [20] + \mathcal{L}_{panoptic} [57] + \mathcal{L}_{semantic} [24] + \mathcal{L}_{depth} [52] + \mathbb{1} \cdot (\mathcal{L}_{dz} [15] + \mathcal{L}_{z_c} + \mathcal{L}_{voxel} [15] + \mathcal{L}_{mesh} [15])$ .

For depth, we use a simple U-Net network structure to predict inverse “stuff” depth, which is adopted from Fac-

tored3D [52] because it is relatively lightweight. In addition to depth, to assist the positioning of objects relative to their environment, we add an inverse z center prediction head to align predicted objects with the predicted layout or depth map in 3D. The z center is defined as  $z_c$  in  $\bar{dz} = \frac{dz}{z_c} \cdot \frac{f}{h}$ , where  $\bar{dz}$  is defined as the scale-normalized depth extent [15],  $h$  is the height of the object’s bounding box,  $f$  is the focal length,  $dz$  is the depth extent. Our z center head predicts the inverse  $z_c$ , which is the object’s center in the z-axis of the camera coordinate system.

In summary, the Panoptic3D (end-to-end) network uses a ResNet and an FPN network as our backbone for detection, along with an FPN-based semantic head to assist the 2D panoptic prediction, an inverse z center head in predicting object centers relative to inverse depth prediction produced by the depth branch, and enables multi-object training and evaluation for the shape heads.

## 4. Datasets

For Panoptic3D (stage-wise), we show qualitative results for natural datasets such as COCO and Cityscapes, where well-annotated panoptic segmentation labels are provided.

To our best knowledge, no available dataset is accurately annotated with amodal instance segmentation, panoptic segmentation, 2.5D information for “stuff”, and 3D meshes for “things”. Most natural image datasets either do not provide panoptic segmentation annotations or suffer from low diversity or low quantity for corresponding 3D mesh annotations. ScanNet [11] has a diverse environment, a large number of images annotated with instance/semantic segmentation, and annotations for corresponding 3D meshes. However, the mesh annotations on ScanNet do not have good alignment with their masks. Additionally, our attempt

Table 2. Available datasets comparison. More comparison is available in [14]. The last row shows the panoptic 3D 3D-FRONT dataset rendered and annotated by us.

Dataset	Instance	Semantic	Panoptic	Depth	3D “things”	3D “stuff”	Alignment
SUN-RGBD [46]	✓	✓	-	✓	0	-	-
AI2Thor [26]	✓	✓	-	✓	100	-	-
ScanNet [11]	✓	✓	-	✓	14225/1160 [2]	-	approx. [2]
3D-FUTURE [14]	✓	-	-	-	9992	-	✓
3D-FRONT [14]	-	-	-	-	9992	✓	✓
Panoptic 3D 3D-FRONT	✓	✓	✓	✓	2717	✓	✓

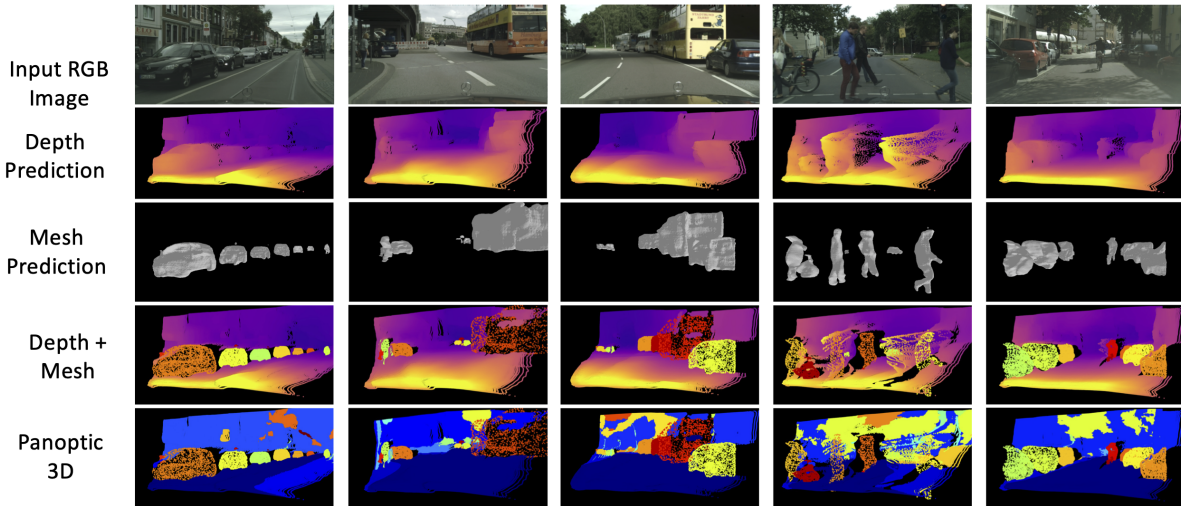


Figure 4. Qualitative results of Panoptic3D (stage-wise) on Cityscapes images [10]. Results are taken from an off-angle shot to show the difference between depth and 3D panoptic results. We sampled the point cloud from the result object meshes for better visualization of the 3D effect. We show that our alignment module outputs visually correct alignment between things reconstruction and “stuff” depth point cloud.

to generate panoptic segmentation information for ScanNet suffers from significant human errors in semantic and instance segmentation annotations. Therefore, we are not able to work on ScanNet for the current end-to-end supervised system. We are also aware of other 3D datasets such as SUN-RGBD [46], AI2Thor [26], Scan2CAD [2], 3D-FUTURE [14] and OpenRooms [31]. We show in Table 2 that the natural datasets, such as SUN-RGBD and ScanNet, do not precisely align 3D “stuff” or “things”. For a virtual dataset, even though we can extract all the information from AI2Thor, the number of shapes was too limited for shape reconstruction training during the early stages of our project. OpenRooms has not yet released its 3D CAD models.

Thanks to the availability of the 3D-FRONT dataset [14], we can generate a first version of the panoptic 3D parsing dataset with COCO-style annotations, including 2D amodal instance and panoptic segmentation, modal and amodal (layout) depth, and corresponding 3D mesh information for every image. Referenced from the 3D-FUTURE dataset [14], we adopt 34 instance categories representing all of the countable objects as “things”, and add three categories rep-

resenting walls, ceilings, and floors as “stuff” as no other “stuff” categories exist in the first release.

For rendering, the first release of the 3D-FRONT dataset does not provide the textures and colors for “stuff” objects, so we adopt textures from the SceneNet RGB-D dataset [37]. We place a point light at the renderer’s camera position for the lightning to make sure the scene is fully lit. We use the official Blender [9] script with the officially released camera angles for this work.

We use the first 1620 houses as the train set and the last 200 houses as the test set for the experiments. We first mark all objects that appear both in the train and test sets as invalid during training, ensuring that the 3D models are disjoint between the train and test sets. We only train and evaluate our mesh prediction on non-boundary (or relatively centered) objects. After filtering out images with no valid things, there are 7734 images in the train set and 1086 in the test set. There are 55216 instances in the train set for the panoptic segmentation task and 7548 instances in the test set. For the 3D reconstruction task, there are 1559 unique models in the train set and 1158 unique models in the test

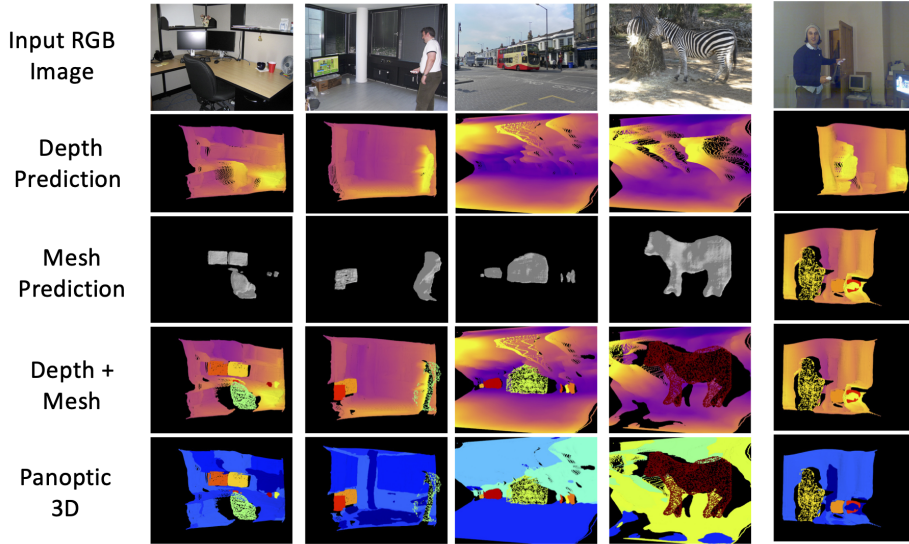


Figure 5. Qualitative results for Panoptic3D (stage-wise) on COCO images [32]. Results are taken from an off-angle shot to show the difference between depth and 3D panoptic results. We sampled the point cloud from the predicted object meshes for better visualization of 3D structures.

set. The final dataset covers 33 categories for “things” during training and 31 types of “things” during evaluation.

## 5. Experiment Details and Evaluation

### 5.1. Stage-wise Panoptic3D

Datasets such as COCO and Cityscapes, have well-annotated panoptic segmentation annotations but lack annotations of 3D shapes and depth information. Figure 2 shows the stage-wise system pipeline. With UPSNet [57] as the backbone, we can use a de-occlusion network [60] for amodal mask prediction and a depth network [1] and an alignment module for scene alignment. Additionally, we use the predicted amodal mask and the input RGB image for unseen class instance reconstruction [61]. The outputs of these networks would then be passed through an alignment module that produces the 3D panoptic parsing results.

For the Cityscapes dataset, we compute its camera intrinsics with  $\text{FOV} = 60$ , height = 1024 and width = 2048 [10]. Since it doesn’t provide camera information for the COCO dataset, we estimate its FOV to be 60 based on heuristics and use an image size of  $480 \times 640$ , which is compatible with every sub-module of the stage-wise system.

In Figure 4 and Figure 5, we show qualitative measures for Cityscapes and COCO, respectively. The pipeline has demonstrated qualitatively good results for both indoor and outdoor natural images.

Using the COCO dataset, we can project the panoptic 3D results back to the input view and evaluate it against their ground truth 2D panoptic annotation to show its image parsing capability. We acquired around 300 images from the

COCO test set that contains overlapped panoptic labels Total3DUnderstanding. In Table 3, we show that our pipeline outperforms Total3DUnderstanding on reprojected panoptic segmentation metrics.

### 5.2. End-to-end Panoptic3D

We train our networks with a learning rate of 0.005 for 30000 iterations. We use PyTorch for code development and 4 GeForce GTX TITAN X GPUs for ablation studies. We switch to 8 GPUs for larger architectures with depth/layout predictions. The experiments with the largest model take 16 hours to run on 8 GeForce GTX TITAN X GPUs. Our input size for the detection backbone is  $1024 \times 1024$  instead of the original  $800 \times 800$  used by Mesh R-CNN because the depth network requires the input to be divisible by 64. The input image is resized to  $512 \times 512$  for the depth branch. The final network contains 13 losses: semantic segmentation pixel-wise classification loss, panoptic segmentation loss, RPN box classification loss, RPN box regression loss, instance box classification loss, instance box regression and segmentation loss, depth extent loss, inverse depth center loss, voxel loss, mesh loss, depth loss, and “stuff” depth loss. Partial loss is used for depth extent, object inverse depth loss, voxel loss, and mesh loss.

### Shape Reconstruction

For the baseline model, we add multi-instance training and allow shape regression only on centered objects on top of detection and reconstruction network structures used in [15]. Ablations on partial-loss training and joint training with other heads are included in Table 4 and Table 5. We

Table 3. Comparison of re-projected 2D panoptic qualities from a subset of COCO indoor images between Total3DUnderstanding and our Panoptic3D (stage-wise) system. For Total3DUnderstanding, the re-projection uses inferred camera extrinsic and we change the predicted layout box into meshes for wall, ceiling, and floor. Our Panoptic3D (stage-wise) method outperforms Total3DUnderstanding on every metrics.

Methods	PQ $\uparrow$			SQ $\uparrow$			RQ $\uparrow$		
	IOU@.5	IOU@.4	IOU@.3	IOU@.5	IOU@.4	IOU@.3	IOU@.5	IOU@.4	IOU@.3
Total3DUnderstanding [38]	0.043	0.06	0.077	0.046	0.063	0.081	0.065	0.101	0.15
Panoptic3D (stage-wise) (ours)	<b>0.168</b>	<b>0.176</b>	<b>0.181</b>	<b>0.177</b>	<b>0.184</b>	<b>0.181</b>	<b>0.21</b>	<b>0.220</b>	<b>0.226</b>

find that utilizing more samples per image for training the instance head can help improve mesh prediction with higher  $AP^{mesh}$  in Table 4. In Table 5, we show that adding additional panoptic, z-center, depth, and layout heads significantly improve the average precision for boxes and masks, but only a slight improvement on meshes when used together. Notice that adding z-center loss starting from the model (b) does not significantly boost the earlier models; however, it provides considerably better qualitative visualization in Figure 6. Compared to row 6 (without z-center loss), row 7 (with z-center loss) shows a more consistent layout against the input RGB image. The furniture cluster around a similar depth in row 6.

Table 4. Baseline model comparisons. Our baseline model (1) is a multi-object training and evaluation enabled detection and reconstruction network [15] trained on centered objects in all three heads (instance, voxel, mesh). Model (2) is the baseline model trained on all things with a partial loss on voxel and mesh heads. N indicates the number of annotations used to regress each corresponding head during training.

Baseline	N instances	N voxels	N meshes	$AP^{box}$	$AP^{mask}$	$AP^{mesh}$
(1)	16175	16175	16175	$37.8 \pm 1.4$	$34.2 \pm 1.9$	$5.9 \pm 0.4$
(2)	55216	16175	16175	$56.5 \pm 0.9$	$52.6 \pm 1.1$	$8.9 \pm 1.5$

Table 5. Ablation studies for the Panoptic3D (end-to-end) model on the panoptic 3D 3D-FRONT dataset. Our ablation study is compared with the baseline (2) in Table 4. The results show that during joint training, the network can maintain its  $AP^{mesh}$  performance while improving on  $AP^{box}$  and  $AP^{mask}$ .

	panoptic	z-center	depth	layout	$AP^{box}$	$AP^{mask}$	$AP^{mesh}$
(2)	-	-	-	-	$56.5 \pm 0.9$	$52.6 \pm 1.1$	$8.9 \pm 1.5$
(a)	✓				$56.7 \pm 2.2$	$55.8 \pm 2.7$	$8.3 \pm 0.6$
(b)	✓	✓			$57.0 \pm 1.7$	$55.5 \pm 1.2$	$8.1 \pm 1.5$
(c)	✓	✓	✓		$59.4 \pm 0.6$	$56.7 \pm 2.4$	$9.0 \pm 1.2$
ours	✓	✓	✓	✓	<b><math>60.0 \pm 1.4</math></b>	<b><math>56.0 \pm 1.4</math></b>	<b><math>9.0 \pm 1.3</math></b>

## Panoptic Segmentation

We compare our panoptic segmentation results with the original UPSNet panoptic segmentation results as one of our baselines. Although we use a panoptic feature pyramid network [24] instead of the FPN network with deformable CNNs from UPSNet, the results are comparable. We notice a slight decrease when we switch masks for instance head

from modal to amodal, as amodal masks may pose challenges to the panoptic head. As for joint training, we show in Table 6 that the results from joint training are comparable with our baseline. We use the metrics of PQ, SQ, and RQ following the panoptic segmentation paper 6.

We are aware that our “stuff” categories are an easy set for panoptic segmentation tasks. 3D-FRONT offers new releases from when we began the project, so for future studies, we will attempt to incorporate more categories, such as doors and windows, with better rendering effects. However, our dataset does provide the first version of any such dataset that enables end-to-end training on the task of panoptic 3D parsing. Based on our acquired results, there are still challenges even with the current “stuff” categories for panoptic segmentation.

Table 6. Ablation studies for the Panoptic3D (end-to-end) model on the panoptic 3D 3D-FRONT dataset. The model numbers here correspond to models in Table 5. Here we show that the panoptic performance is comparable to the baseline performance with joint training.

	panoptic	z-center	depth	layout	PQ	SQ	RQ
(a)	✓				46.4	76.8	54.0
(b)	✓	✓			46.0	75.9	53.4
(c)	✓	✓	✓		47.4	76.1	55.2
ours	✓	✓	✓	✓	46.9	75.7	54.4

## Depth and Layout predictions

We adopt the U-Net structure from Factored3D and jointly train the depth with the rest of our pipeline. We find regressing for layout depth alone is an easier task for the network than joint training. Joint training using layout depth loss with other losses appear to be a challenging problem. Adding cross-consistency loss [59] between layout depth and normal does not seem to improve depth’s performance easily. Nonetheless, adding layout depth loss appears to help the network to perform better in general in both shape metrics and panoptic metrics as shown in Table 5 and Table 6.

## 6. Conclusions

This paper presents a framework that aims towards tackling panoptic 3D parsing for a single image in the wild. We demonstrate qualitative results for natural images from

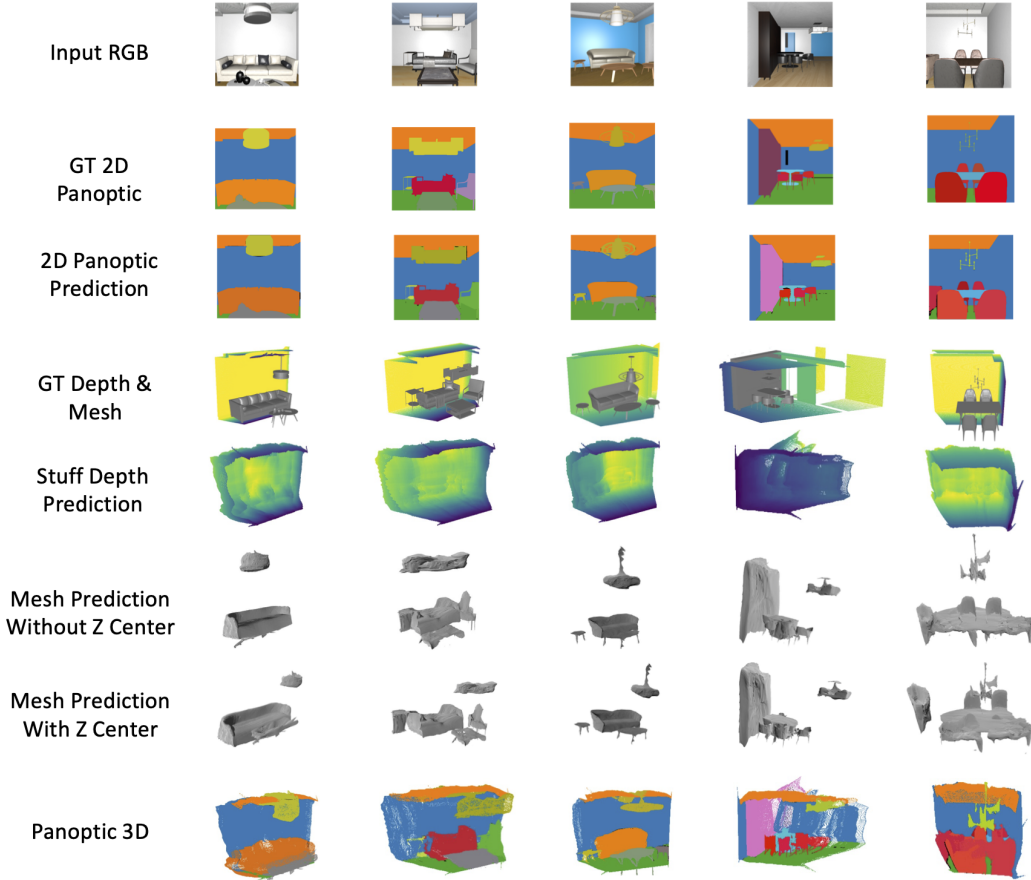


Figure 6. Qualitative results for Panoptic3D (end-to-end) on the 3D-FRONT dataset [14]. We show our predicted panoptic results (row 3) compared to panoptic ground truth (row 2) and our reconstruction results (row 5 to 7) to reconstruction ground truth (row 4). Row 8 shows the final panoptic 3D results, where we sample point clouds from meshes for better visualization. Comparing rows 6 and 7, row 7 shows the object placement is more consistent with the input RGB image. Our final results show that the shape predictions align well with the predicted “stuff” depth prediction.

datasets such as Cityscapes [10] (shown in Figure 4) and COCO [32] (shown in Figure 5) under the stage-wise system. Additionally, an end-to-end pipeline that can be trained with full annotations is also proposed.

For societal impact, we are proposing a new task in computer vision, Panoptic 3D Parsing (Panoptic3D), that is concerned with a central task in computer vision: joint single image foreground object detection and segmentation, background semantic labeling, depth estimation, 3D reconstruction, and 3D layout estimation. A successful Panoptic3D system can see its applications in a wide range of domains beyond computer vision such as mapping, transportation, computer graphics etc. However, Panoptic3D is a learning based system and may have bias introduced in various training stages. Careful justification and adoption of the system in appropriate tasks subject to regulation are needed.

**Limitations:** We use a fixed FOV of 60 and fixed image

sizes for Cityscapes, COCO, and 3D-FRONT. Hence the estimated 3D scene can only provide a rough ordering estimation of things and stuff in terms of distance to the camera plane. We use a single light source for the 3D-FRONT image rendering, which results in artificial lighting for the training images. Therefore, the generalization capability for the models trained using this dataset might not be strong. We expect the model to generalize better under more natural lighting conditions, which is to be verified in the next step with a new dataset.

## 7. Acknowledgments

Part of the work was done during Sainan Liu’s internship at Intel.

## References

- [1] Ibraheem Alhashim and Peter Wonka. High quality monocular depth estimation via transfer learning. *arXiv e-prints*, abs/1812.11941, 2018. 1, 2, 3, 6
- [2] Armen Avetisyan, Manuel Dahnert, Angela Dai, Manolis Savva, Angel X. Chang, and Matthias Niessner. Scan2cad: Learning cad model alignment in rgb-d scans. *CVPR*, June 2019. 5
- [3] Aayush Bansal, Bryan C. Russell, and Abhinav Gupta. Marr revisited: 2D-3D alignment via surface normal prediction. *CVPR*, 2016. 2
- [4] Myron Z Brown, Darius Burschka, and Gregory D Hager. Advances in computational stereo. *IEEE TPAMI*, 25(8):993–1008, 2003. 2
- [5] Angel X. Chang, A. Thomas Funkhouser, Leonidas J. Guibas, Pat Hanrahan, Qi-xing Huang, Zimo Li, Silvio Savarese, Manolis Savva, Shuran Song, Hao Su, Jianxiang Xiao, Li Yi, and Fisher Yu. ShapeNet: An information-rich 3D model repository. *CoRR 1512.03012*, 2015. 1
- [6] Qimin Chen, Vincent Nguyen, Feng Han, Raimondas Kiveris, and Zhuowen Tu. Topology-aware single-image 3D shape reconstruction. *CVPR Workshop on Learning 3D Generative Models*, 2020. 2
- [7] Zhiqin Chen and Hao Zhang. Learning implicit fields for generative shape modeling. In *CVPR*, 2019. 2
- [8] Ismael Colomina and Pere Molina. Unmanned aerial systems for photogrammetry and remote sensing: A review. *ISPRS Journal of photogrammetry and remote sensing*, 92:79–97, 2014. 2
- [9] Blender Online Community. *Blender - a 3D modelling and rendering package*. Blender Foundation, Stichting Blender Foundation, Amsterdam, 2018. 5
- [10] Marius Cordts, Mohamed Omran, Sebastian Ramos, Timo Rehfeld, Markus Enzweiler, Rodrigo Benenson, Uwe Franke, Stefan Roth, and Bernt Schiele. The cityscapes dataset for semantic urban scene understanding. *CVPR*, 2016. 1, 2, 3, 5, 6, 8
- [11] Angela Dai, Angel X. Chang, Manolis Savva, Maciej Halber, Thomas Funkhouser, and Matthias Nießner. ScanNet: Richly-annotated 3D reconstructions of indoor scenes. *CVPR*, 2017. 4, 5
- [12] Jia Deng, Wei Dong, Richard Socher, Li-Jia Li, Kai Li, and Li Fei-Fei. Imagenet: A large-scale hierarchical image database. *CVPR*, pages 248–255, 2009. 1
- [13] David Eigen, Christian Puhrsch, and Rob Fergus. Depth map prediction from a single image using a multi-scale deep network. *NeurIPS*, 2014. 2
- [14] Huan Fu, Rongfei Jia, Lin Gao, Mingming Gong, Bin-qiang Zhao, Steve Maybank, and Dacheng Tao. 3D-FUTURE: 3D furniture shape with texture. *arXiv preprint arXiv:2009.09633*, 2020. 1, 2, 5, 8
- [15] Georgia Gkioxari, Jitendra Malik, and Justin Johnson. Mesh R-CNN. *ICCV*, 2019. 1, 2, 4, 6, 7
- [16] Ian Goodfellow, Yoshua Bengio, and Aaron Courville. *Deep learning*, volume 1. MIT Press, 2016. 1
- [17] Thibault Groueix, Matthew Fisher, Vladimir G. Kim, Bryan Russell, and Mathieu Aubry. AtlasNet: A Papier-Mâché Approach to Learning 3D Surface Generation. *CVPR*, 2018. 2
- [18] Feng Han and Song-Chun Zhu. Automatic single view building reconstruction by integrating segmentation. In *2004 Conference on Computer Vision and Pattern Recognition Workshop*, pages 53–53, 2004. 2
- [19] Richard Hartley and Andrew Zisserman. *Multiple view geometry in computer vision*. Cambridge university press, 2003. 2
- [20] Kaiming He, Georgia Gkioxari, Piotr Dollár, and Ross Girshick. Mask R-CNN. *ICCV*, 2017. 1, 4
- [21] Kaiming He, Xiangyu Zhang, Shaoqing Ren, and Jian Sun. Deep residual learning for image recognition. *CVPR*, 2016. 1
- [22] Siyuan Huang, Siyuan Qi, Yinxue Xiao, Yixin Zhu, Ying Nian Wu, and Song-Chun Zhu. Cooperative holistic scene understanding: Unifying 3D object, layout, and camera pose estimation. *NeurIPS*, pages 206–217, 2018. 2
- [23] Angjoo Kanazawa, Michael J Black, David W Jacobs, and Jitendra Malik. End-to-end recovery of human shape and pose. *CVPR*, 2018. 2
- [24] Alexander Kirillov, Ross B. Girshick, Kaiming He, and Piotr Dollár. Panoptic feature pyramid networks. *CVPR*, 2019. 2, 4, 7
- [25] Alexander Kirillov, Kaiming He, Ross B. Girshick, Carsten Rother, and Piotr Dollár. Panoptic Segmentation. *CVPR*, 2018. 1, 2, 3
- [26] Eric Kolve, Roozbeh Mottaghi, Winson Han, Eli VanderBilt, Luca Weihs, Alvaro Herrasti, Daniel Gordon, Yuke Zhu, Abhinav Gupta, and Ali Farhadi. AI2-THOR: An Interactive 3D Environment for Visual AI. *ArXiv*, abs/1712.05474, 2017. 5
- [27] Alex Krizhevsky, Ilya Sutskever, and Geoffrey E Hinton. ImageNet classification with deep convolutional neural networks. *NeurIPS*, 2012. 1
- [28] Kiriakos N Kutulakos and Steven M Seitz. A theory of shape by space carving. *International journal of computer vision*, 38(3):199–218, 2000. 2
- [29] Justin Lazarow, Kwonjoon Lee, and Zhuowen Tu. Learning instance occlusion for panoptic segmentation. *CVPR*, 2019. 2
- [30] Zhengqi Li and Noah Snavely. MegaDepth: Learning single-view depth prediction from internet photos. *CVPR*, 2018. 1, 2
- [31] Zhengqin Li, Ting Yu, Shen Sang, Sarah Wang, Sai Bi, Zexiang Xu, Hong-Xing Yu, Kalyan Sunkavalli, Milovs Havsan, Ravi Ramamoorthi, and Manmohan Chandraker. Openrooms: An end-to-end open framework for photorealistic indoor scene datasets. *CVPR*, abs/2007.12868, 2021. 5
- [32] Tsung-Yi Lin, Michael Maire, Serge J. Belongie, James Hays, Pietro Perona, Deva Ramanan, Piotr Dollár, and C. Lawrence Zitnick. Microsoft COCO: Common objects in context. *ECCV*, 2014. 1, 2, 3, 6, 8
- [33] Wilfried Linder. *Digital photogrammetry*. Springer, 2009. 2
- [34] Jonathan Long, Evan Shelhamer, and Trevor Darrell. Fully convolutional networks for semantic segmentation. *CVPR*, 2015. 1, 2

- [35] Yi Ma, Stefano Soatto, Jana Kosecka, and S Shankar Sastry. *An invitation to 3-d vision: from images to geometric models*, volume 26. Springer, 2012. [2](#)
- [36] David Marr. *Vision: A Computational Investigation into the Human Representation and Processing of Visual Information*. Henry Holt and Co., Inc., USA, 1982. [1](#), [2](#)
- [37] John McCormac, Ankur Handa, Stefan Leutenegger, and Andrew J. Davison. SceneNet RGB-D: Can 5m synthetic images beat generic imagenet pre-training on indoor segmentation? *ICCV*, 2017. [5](#)
- [38] Yinyu Nie, Xiaoguang Han, Shihui Guo, Yujian Zheng, Jian Chang, and Jian Jun Zhang. Total3DUnderstanding: Joint layout, object pose and mesh reconstruction for indoor scenes from a single image. *CVPR*, June 2020. [1](#), [2](#), [7](#)
- [39] Marc Pollefeys, Reinhard Koch, and Luc Van Gool. Self-calibration and metric reconstruction inspite of varying and unknown intrinsic camera parameters. *International Journal of Computer Vision*, 32(1):7–25, 1999. [2](#)
- [40] Marc Pollefeys, David Nistér, J-M Frahm, Amir Akbarzadeh, Philippos Mordohai, Brian Clipp, Chris Engels, David Gallup, S-J Kim, Paul Merrell, et al. Detailed real-time urban 3D reconstruction from video. *International Journal of Computer Vision*, 78(2-3):143–167, 2008. [2](#)
- [41] Shaoqing Ren, Kaiming He, Ross B. Girshick, and Jian Sun. Faster R-CNN: Towards real-time object detection with region proposal networks. *NeurIPS*, 2015. [1](#)
- [42] Lawrence G Roberts. *Machine perception of three-dimensional solids*. PhD thesis, Massachusetts Institute of Technology, 1963. [2](#)
- [43] Ashutosh Saxena, Min Sun, and Andrew Y. Ng. Make3D: Learning 3D scene structure from a single still image. *IEEE TPAMI*, 2009. [2](#)
- [44] Jamie Shotton, John Winn, Carsten Rother, and Antonio Criminisi. Textonboost: Joint appearance, shape and context modeling for multi-class object recognition and segmentation. In *ECCV*, 2006. [1](#)
- [45] Karen Simonyan and Andrew Zisserman. Very deep convolutional networks for large-scale image recognition. In *ICLR*, 2015. [1](#)
- [46] Shuran Song, Samuel P. Lichtenberg, and Jianxiong Xiao. SUN RGB-D: A RGB-D scene understanding benchmark suite. *CVPR*, 2015. [5](#)
- [47] Christian Szegedy, Wei Liu, Yangqing Jia, Pierre Sermanet, Scott Reed, Dragomir Anguelov, Dumitru Erhan, Vincent Vanhoucke, and Andrew Rabinovich. Going deeper with convolutions. In *CVPR*, 2015. [1](#)
- [48] Richard Szeliski. *Computer vision: algorithms and applications*. Springer Science & Business Media, 2010. [2](#)
- [49] Michael J Tarr and Quoc C Vuong. Visual object recognition. *Stevens' handbook of experimental psychology*, 2002. [1](#)
- [50] Zhuowen Tu. Auto-context and its application to high-level vision tasks. In *CVPR*, 2008. [1](#)
- [51] Zhuowen Tu, Xiangrong Chen, Alan L Yuille, and Song-Chun Zhu. Image parsing: Unifying segmentation, detection, and recognition. *IJCV*, 63(2):113–140, 2005. [1](#), [2](#), [3](#)
- [52] Shubham Tulsiani, Saurabh Gupta, David Fouhey, Alexei A. Efros, and Jitendra Malik. Factoring shape, pose, and layout from the 2D image of a 3D scene. *CVPR*, 2018. [1](#), [2](#), [4](#)
- [53] Shimon Ullman. The interpretation of structure from motion. *Proceedings of the Royal Society of London. Series B. Biological Sciences*, 203(1153):405–426, 1979. [2](#)
- [54] Nanyang Wang, Yinda Zhang, Zhuwen Li, Yanwei Fu, Wei Liu, and Yu-Gang Jiang. Pixel2mesh: Generating 3D mesh models from single rgb images. *ECCV*, 2018. [2](#)
- [55] Zhirong Wu, Shuran Song, Aditya Khosla, Fisher Yu, Linguang Zhang, Xiaoou Tang, and Jianxiong Xiao. 3D shapenets: A deep representation for volumetric shapes. *CVPR*, 2015. [2](#)
- [56] Saining Xie, Ross Girshick, Piotr Dollár, Zhuowen Tu, and Kaiming He. Aggregated residual transformations for deep neural networks. *CVPR*, 2017. [1](#)
- [57] Yuwen Xiong, Renjie Liao, Hengshuang Zhao, Rui Hu, Min Bai, Ersin Yumer, and Raquel Urtasun. UPSNet: A unified panoptic segmentation network. *CVPR*, 2019. [2](#), [3](#), [4](#), [6](#)
- [58] Qiangeng Xu, Weiyue Wang, Duygu Ceylan, Radomir Mech, and Ulrich Neumann. Disn: Deep implicit surface network for high-quality single-view 3D reconstruction. *NeurIPS*, pages 492–502, 2019. [2](#)
- [59] Amir Zamir, Alexander Sax, Teresa Yeo, Oğuzhan Kar, Nikhil Cheerla, Rohan Suri, Zhangjie Cao, Jitendra Malik, and Leonidas Guibas. Robust learning through cross-task consistency. *CVPR*, 2020. [7](#)
- [60] Xiaohang Zhan, Xingang Pan, Bo Dai, Ziwei Liu, Dahua Lin, and Chen Change Loy. Self-supervised scene deocclusion. *CVPR*, June 2020. [3](#), [6](#)
- [61] Xiuming Zhang, Zhoutong Zhang, Chengkai Zhang, Joshua B Tenenbaum, William T Freeman, and Jiajun Wu. Learning to reconstruct shapes from unseen classes. *NeurIPS*, 2018. [1](#), [2](#), [3](#), [6](#)
- [62] Chuhan Zou, Alex Colburn, Qi Shan, and Derek Hoiem. Layoutnet: Reconstructing the 3D room layout from a single rgb image. *CVPR*, 2018. [2](#)